Research Square

Preprints are preliminary reports that have not undergone peer review.
They should not be considered conclusive, used to inform clinical practice,
or referenced by the media as validated information.

Comparative characterization of α-Synuclein ligands for off-target binding to monoamine oxidase-B

Magdalena. Wadsak
University of Bern: Universitat Bern
Quanling Jiang
University of Bern: Universitat Bern
Shixiang Zhang
Fudan University
Deborah Gozzi
University of Bern: Universitat Bern
Feng-Tao Liu
Huashan Hospital Fudan University
Kuangyu Shi
University of Bern: Universitat Bern
Axel Rominger
Inselspital University Hospital Bern: Inselspital Universitatsspital Bern
Jian Wang
Huashan Hospital Fudan University
Chuantao Zuo
Huashan Hospital Fudan University
Ruiqing Ni
ruiqing.ni@unibe.ch

University of Bern: Universitat Bern https://orcid.org/0000-0002-0793-2113

Short Report

Keywords: alpha-synuclein, Parkinson's disease, PET, MAO-B, off-target, Multiple System Atrophy

Posted Date: November 24th, 2026

DOI: https://doi.org/10.21203/rs.3.rs-11702901/v1

License: This work is licensed under a Creative Commons Attribution 4.0 International License.
Read Full License

Comparative characterization of α-Synuclein ligands for off-target binding to monoamine oxidase-B

Magdalena Wadsak[1,2#], Quanling Jiang[1,3#], Shixiang Zhang[3#], Deborah Gozzi[1], Feng-Tao Liu[4], Kuangyu Shi[1], Axel Rominger[1], Jian Wang[4*], Chuantao Zuo[3*], Ruiqing Ni[1,5*]

[1]Department of Nuclear Medicine, Inselspital, University of Bern, Bern, Switzerland;

[2]Graduate School of Cellular and Biomedical Sciences, University of Bern, Bern, Switzerland

[3]Department of Nuclear Medicine/PET Center, Huashan Hospital, Fudan University, Shanghai, China;

[4]Department of Neurology and National Research Center for Aging and Medicine & National Center for Neurological Disorders, State Key Laboratory of Medical Neurobiology, Huashan Hospital, Fudan University, Shanghai, China;

[5]Institute for Regenerative Medicine, University of Zurich, Zurich, Switzerland;

#Co-first author

*Corresponding author

Ruiqing Ni

Email: ruiqing.ni@unibe.ch

Address: Department of Nuclear Medicine, Inselspital & University of Bern, Rosenbühlgasse 25, 3010 Bern, Switzerland

Chuantao Zuo

Email: zuochuantao@fudan.edu.cn

Address: Department of Nuclear Medicine/PET Center, Huashan Hospital, Fudan University, Shanghai, China; 518 East Wuzhong RD, 200040 Shanghai, China

Jian Wang

Email: wangjian_hs@fudan.edu.cn

Address: Department of Nuclear Medicine/PET Center, Huashan Hospital, Fudan University, Shanghai, China; 518 East Wuzhong RD, 200040 Shanghai, China

Abstract

Background

Reliable *in vivo* visualization of alpha-synuclein (α-syn) aggregates is essential for studying synucleinopathies such as multiple system atrophy and Parkinson's disease. However, the potential off-target binding of candidate tracers such as monoamine oxidase B (MAO-B) remains a major concern. This study aimed to determine the off-target binding profile of α-syn probes using postmortem human brain tissue and *in vivo* imaging.

Methods

High-resolution autoradiography using [^{3}H]L-deprenyl (targeting MAO-B) was performed with different concentrations of MODAG-009, MODAG-005, anle138b, C05-05, FD4, and ACI-12589 on frozen postmortem human brain cortical tissue. Immunofluorescence staining was performed using antibodies against MAO-B to validate the targets. *In vivo* [^{18}F]FD4 PET in a multiple system atrophy patient was performed before and after chronic treatment with the MAO-B inhibitor rasagiline (1 mg/day).

Results

MODAG-009, MODAG-005 and anle138b reduced [^{3}H]L-deprenyl binding by approximately 86%, 77%, and 31%, respectively, indicating off-target binding to MAO-B (Ki= 216 nM, 204 nM and 64 nM, respectively). ACI-12589 displaced approximately 50% of [^{3}H]L-deprenyl binding, with a Ki= 368 nM. In contrast, FD4 and C05-05 showed almost no off-target binding to MAO-B. Repeated *in vivo* [^{18}F]FD4 PET in the multiple system atrophy patient revealed no competition between rasagiline and [^{18}F]FD4.

Conclusions

In vivo and *in vitro* evidence indicated that different off-target binding patterns of different α-syn probes to MAO-B were observed. This finding provides mechanistic insight into the potential signal origin of α-syn PET and underscores the value of validation in tracer development.

Keywords:

alpha-synuclein, Parkinson's disease, PET, MAO-B, off-target, Multiple System Atrophy

Introduction

α-Synucleinopathy is characterized by the accumulation of alpha-synuclein (αSyn) in Parkinson's disease (PD), dementia with Lewy bodies (DLB) and multiple system atrophy (MSA). The abnormal cerebral accumulation and spread of pathological protein aggregates affect select vulnerable circuits in a disease-specific pattern[1]. Early diagnosis of synucleinopathies remains challenging, as motor symptoms typically appear only after substantial neuronal loss, and clinical overlap among PD, DLB, and MSA complicates differential diagnosis[2, 3]. Biomarkers for detecting αSyn at an early stage represent a tremendous unmet clinical need. The use of positron emission tomography (PET) with amyloid-beta and tau ligands has facilitated the early diagnosis of Alzheimer's disease[4]. Currently, there several PET ligands of different scaffolds for αSyn aggregates under development at different phases[5], e.g., [^{18}F]ACI-12589[6], [^{18}F]ACI-15916 (NCT06891703), [^{18}F]F0502B[7], [^{11}C]MODAG-005[8], [^{18}F]MODAG-009 (NCT07640555), [^{18}F]C05-05[9], [^{18}F]SPAL-T-06[10], [^{18}F]FD4[11] (NCT07253753), [^{18}F]FD17 (NCT06738862) and [^{18}F]UCB-2897 (NCT05274568), [^{11}C]M503-1619[12] and [^{11}C]SY08 (NCT06098612), [^{11}C]M503-1619[12, 13]. An earlier study revealed that [^{18}F]ACI-12589[6] had high-affinity binding and specificity for pathological αSyn and enabled clear differentiation of MSA patients from healthy controls and patients with other neurodegenerative disorders. However, [^{18}F]ACI-12589 showed limited retention in PD and DLB, likely reflecting the lower aggregate density or distinct fibril conformations in these diseases.

αSyn remains the most difficult of the major neurodegenerative proteinopathies to image selectively: unlike Aβ and tau, no αSyn PET ligand has yet demonstrated fully selective binding in humans, and virtually every candidate tracer characterized to date, e.g., off-target signals, e.g., to the choroid plexus (via TMEM106B amyloid) or to white matter, to amyloid-beta or to tau[14, 15]. αSyn pathology, such as tau pathology, is frequently accompanied by reactive astrogliosis. With respect to tau tracers, the off-target binding of MAO-B has repeatedly emerged among structurally diverse tracers.

The aim of this study was to investigate the off-target binding of αSyn ligands to MAO-B. Direct *in vitro* comparison of MODAG-009, MODAG-005, C05-05, ACI-12589 and FD4 for the off-target

binding of MAO-B using a competition autoradiography assay was performed *in vitro*, and the results were further confirmed by *in vivo* [^{18}F]FD4 imaging in patients with chronic treatment with rasagiline.

Methods

Chemicals

The chemical compounds FD4, 1-fluoro-3-((2-((E)-2-(6'-(methylamino)-[3,3'-bipyridin]-6-yl)vinyl)benzo[d]thiazol-5-yl)oxy)propan-2-ol; ACI-12589, 2-(6-((R)-3-fluoropyrrolidin-1-yl)pyridin-3-yl)-5-(pyridin-3-yl)-5,6-dihydropyrrolo[3,4-c]pyrazol-4(2H)-one; C05-05, 1-fluoro-3-((2-((E)-4-(6-(methylamino)pyridin-3-yl)but-1-en-3-yn-1-yl)benzo[d]thiazol-5-yl)oxy)propan-2-ol; and MODAG-9, 4-(3-(2-fluoropyridin-4-yl)-1H-pyrazol-5-yl)-N-methylaniline (**Fig. 1a**) were synthesized and provided by Shixiang Zhang, Fudan University. All the other chemicals, including MODAG-005, 4-(3-(2-bromopyridin-4-yl)-1H-pyrazol-5-yl)-N-methylaniline (Cat. No. HY-184511; **Fig. 1a**), R-(-)-deprenyl hydrochloride (Cat. No. M003-250MG) and anle138b (Cat. No. SML1515-5MG), were purchased from Sigma Aldrich. [^{3}H]L-deprenyl (83 Ci/mmol, 38 MBq/mL; radiochemical purity >99%) was purchased from Novandi Chemistry Sodertalje, Sweden.

Postmortem human brain tissue

Postmortem human frontal cortex tissue from five patients, including four females and one male whose mean age at death was 83.4 ± 6.6 years (range: 75–92 years), was used for *in vitro* autoradiography experiments. The mean postmortem delay was 4.77 ± 0.53 h. Tissue samples were obtained from the Netherlands Brain Bank (NBB). All tissue samples were collected from donors who provided written informed consent for brain autopsy and for the use of the materials and associated clinical information in research, as coordinated by the NBB. The study followed the principles of the Declaration of Helsinki and its successive revisions. Ethical approval for the use of human brain tissue was obtained from the regional human ethics committee and the medical ethics committee of the VU Medical Center. Frozen tissue samples were stored at -80°C until sectioning.

In vitro autoradiography

In vitro autoradiography was performed using [^{3}H]L-deprenyl [16, 17], a high-affinity, irreversible MAO-B radioligand, to assess displacement by selected compounds in postmortem frontal cortex tissue (n=5) as described earlier [17, 18]. The frozen sections were air-dried and preincubated for 15 min in 0.05 M sodium-potassium phosphate buffer (NaK-PB; pH 7.4) and then incubated for 60 min at room temperature with 10 nM [^{3}H]L-deprenyl. Total binding was defined as the absence of a competing ligand. For competition, sections were coincubated with 10 nM [^{3}H]L-deprenyl and 1 μM of one of the following: unlabeled R-(.-)-deprenyl hydrochloride, FD4, C05-05, ACI-12589, anle138b, MODAG-009, or MODAG-005. For the displacement assay to further compute the Ki, postmortem frontal cortex tissue (n = 3) was used. Different concentrations of ACI-12589, anle138b, MODAG-009, or MODAG-005 (0.1 nM–10 μM) were used, with different concentrations of unlabeled R-(-)-deprenyl hydrochloride used as a reference.

Following incubation, the sections were washed twice in ice-cold Na-K phosphate buffer for 2 minutes and briefly rinsed in ice-cold deionized water. Sections were air-dried overnight and exposed to tritium-sensitive imaging plates (28956482, Amersham BAS-IP TR 2025, Cytiva) for 1 week together with calibrated tritium standards (ART 0123 and ART 0123B, American Radiolabeled Chemicals, St. Louis, MO, USA). Imaging plates were subsequently scanned using an Amersham Typhoon scanner (Cytiva) at 10 μm resolution, and autoradiographic images were analyzed using Fiji (ImageJ).

Quantification

Autoradiographic images were quantified using Fiji/ImageJ. Regions of interest (ROIs) were manually drawn around the entire tissue section and separated into grey and white matter. The mean gray values were converted to radioactivity (nCi/mg) using calibration curves generated from tritium standards exposed alongside the tissue sections. Standard activities were corrected for radioactive decay to the experimental date using a tritium half-life of 12.32 years. Background correction was applied consistently to both tissue measurements and calibration standards. For comparison across experimental conditions, the radioactivity values were normalized to the corresponding total binding and expressed as a percentage of total binding.

Concentration-dependent inhibition of [^{3}H]L-deprenyl binding was analyzed using nonlinear regression with a one-site competitive binding model (one site–fit K_i) [19] in GraphPad Prism 11. The radioligand concentration and dissociation constant were both set to 10 nM. The upper and lower plateaus were constrained to values less than 100% and greater than 0%, respectively. The K_i value and goodness of fit were calculated.

Staining and microscopy

MAO-B immunofluorescence staining was performed on postmortem frontal cortex tissue slices adjacent to the tissue used for autoradiography for comparison. Freshly frozen cryosections were air-dried at room temperature for 5–20 min. The tissue sections were subsequently fixed in 4% formaldehyde in phosphate-buffered saline (PBS, pH 7.4) for 15 min at room temperature (RT). Following fixation, the sections were washed with PBS for 3×5 min at RT. Antigen retrieval was performed in citrate buffer at RT for 20 min, followed by washing with PBS for 3×5 min under mild shaking. Blocking of nonspecific binding was blocked using 5% normal donkey serum (NDS) in 1% Triton-PBS for 1 h at RT in a humid chamber. The sections were then incubated with the primary antibody anti-MAO-B (1:500; Santa Cruz Biotec sc-515354; mouse)[19] in 3% NDS in Triton-PBS (0.3% Triton) overnight at 4 °C. The following day, the samples were washed in PBS and incubated with the corresponding secondary antibody, Alexa488-conjugated anti-mouse *IgG* (1:500; Jackson 715–545–151; donkey), in PBST (0.3% Triton) for 2 h at RT in a humid chamber. The samples were then washed with PBS for 3×5 min in the dark. The sections were incubated for 15 min in the dark with 4′,6-diamidino 2-fenylindol (DAPI, 1:1000) and then were washed with PBS for 2×10 min, after which the coverslips were mounted with ProLong™ Diamond Antifade Mounting (Invitrogen, P36961). The images were acquired with a Slide Scanner Panoramic 250 Flash II (3DHistech, Hungary) and a Ti2 CrEST V3 DeepSIM confocal microscope (Nikon, Japan).

[^{18}F]FD4 PET and magnetic resonance imaging (MRI)

Participants: Between August and September 2025, one participant with MSA was prospectively recruited from the Movement Disorders Clinic, Department of Neurology, Huashan Hospital, Fudan University, Shanghai, China. MSA was diagnosed according to the 2022 Movement Disorder Society (MDS) criteria[20]. The patient underwent a comprehensive neurological assessment by a movement disorder specialist at Huashan Hospital and completed baseline [^{18}F]FD4 PET and structural MRI before the initiation of rasagiline treatment. Following the baseline imaging examination, the patient underwent a 1-month chronic rasagiline challenge (1 mg once daily) and subsequently underwent repeated [^{18}F]FD4 PET and structural MRI examinations. The study was registered with the Chinese Clinical Trial Registry (ChiCTR2400093084) and approved by the Ethics Committee of Huashan Hospital, Fudan University (number: KY2024-1241). Written informed consent was obtained from the patient before enrollment. All study procedures were conducted in accordance with the ethical principles of the Declaration of Helsinki.

[^{18}F]FD4 PET image acquisition: [^{18}F]FD4 PET/CT scans were acquired at Huashan Hospital using a uMI 780 PET/CT scanner (United Imaging Healthcare, Shanghai, China). A low-dose CT scan was first acquired for attenuation correction (10 s). The participant received an intravenous injection of 300 MBq (±10%) of [^{18}F]FD4, and PET acquisition was initiated 60–80 minutes after tracer administration. PET images were reconstructed using the built-in ordered subset expectation maximization (OSEM) algorithm with 4 iterations and 20 subsets, yielding a matrix size of 192 × 192 × 183 and a voxel size of 1.56 × 1.56 × 1.63 mm^3. Structural T1-weighted MR images were acquired using a uPMR 790 T PET/MR scanner (United Imaging Healthcare, Shanghai, China). High-resolution T1-weighted anatomical images were acquired using a 3-dimensional fast gradient-echo sequence with the following parameters: repetition time = 7.9 ms, echo time = 3.0 ms, inversion time = 750 ms, flip angle = 10°, bandwidth = 250 Hz/pixel, matrix size = 230 × 256, voxel size = 1.00 × 1.00 × 1.00 mm^3, and slice thickness = 1 mm. The total acquisition time for the T1-weighted sequence was 4 min 20 s. The same PET and MRI acquisition protocols were used at baseline and after 1 month of rasagiline treatment. PET and MR images were visually inspected before further preprocessing and analysis to exclude apparent motion artifacts and assess overall image quality.

[^{18}F]FD4 PET image processing and analysis: PET image preprocessing and regional quantification were performed using MATLAB R2018b (MathWorks, Natick, MA, USA) and SPM12 (Wellcome Trust Centre for Neuroimaging, London, UK). The [^{18}F]FD4 PET images was rigidly coregistered to the corresponding individual T1-weighted MR images, which served as the anatomical reference for subsequent image processing and regional quantification. Regional [^{18}F]FD4 uptake was quantified as standardized uptake value ratios (SUVRs), with cerebellar gray matter used as the reference region. The cerebellar gray matter reference region and predefined regions of interest (ROIs) were obtained from anatomical atlases, including the Automated Anatomical Labeling atlas 3 (AAL3), MNI PD25 atlas[21], and PMOD-defined anatomical templates. Regional SUVRs were calculated for the predefined ROIs for both baseline and post-rasagiline PET scans.

For visual assessment, baseline and postrasagiline [^{18}F]FD4 PET images and the corresponding SUVR images were visualized using PMOD 4.0 (PMOD Technologies LLC, Zurich, Switzerland), with the individual T1-weighted MR images serving as the anatomical reference. The spatial distribution and regional intensity of [^{18}F]FD4 retention were visually compared between baseline and post-rasagiline scans.

To further facilitate direct comparison, a subtraction image was generated for the participant by digitally subtracting the baseline SUVR image from the corresponding postrasagiline SUVR image (postrasagiline minus baseline). The same display settings were applied to the paired SUVR images and subtraction images for visual comparison. The percentage change in regional [^{18}F]FD4 SUVR following 1 month of rasagiline treatment was calculated as follows:

$$\text{Change (\%)} = \frac{\text{Post-rasagiline SUVR-Baseline SUVR}}{\text{Baseline SUVR}} \times 100\%$$

Negative values indicated decreased regional [^{18}F]FD4 retention after rasagiline treatment, whereas positive values indicated increased retention.

Statistics

Statistical analyses were performed in GraphPad Prism 11 using one-way repeated-measures ANOVA (Geisser–Greenhouse correction, no sphericity assumption), with Dunnett's multiple-comparisons test used to compare each competition condition against the total condition. Multiplicity-adjusted P values are reported; $P < 0.05$ was considered to indicate statistical significance. The error bars indicate the standard deviation (SD). The values represent the mean ± standard deviation (SD).

Results

Divergent binding patterns of αSyn ligands to MAO-B

We first screened the potential off-target binding of different ligands to MAO-B by [^{3}H]L-deprenyl autoradiography of the postmortem human brain (n = 5; **Fig 1a**). Both diarylpyrazole-based compounds, MODAG-009 and MODAG-005, effectively displaced [^{3}H]L-deprenyl binding by 86% and 77% of the total binding (at 1 μM), respectively. Both reductions were significantly different from total [^{3}H]L-deprenyl binding ($p = 0.0066$ and $p = 0.0437$, respectively) and were comparable to the displacement achieved by unlabeled R-(-)-deprenyl hydrochloride (1 μM). In contrast, anle138b (1 μM) reduced [^{3}H]L-deprenyl binding to only approximately 31%. In contrast, FD4 (at 1 μM) or C05-05 (at 1 μM) did not displace [^{3}H]L-deprenyl binding (less than approximately 5% reduction) and are therefore unlikely to interact with MAO-B. ACI-12589 (at 1 μM) displaced approximately 50% of [^{3}H]L-deprenyl, which was not significantly different from total [^{3}H]L-deprenyl binding ($p = 0.0685$) (**Fig 1b, c**). These findings indicate a common off-target affinity of this diarylpyrazole scaffold for MAO-B.

In addition, MAO-B staining was performed on adjacent tissue slices to validate the target (**Fig. 1d, SFig. 1**). MAO-B signals in gray matter as well as in white matter astrocytes were observed. The displacement of diarylpyrazole scaffold compounds to [^{3}H]L-deprenyl occurs both in gray matter and in white matter (**Fig 1b, SFig 2**).

The diarylpyrazole scaffold compounds MODAG-009, MODAG-005, and anle138b showed off-target binding to MAO-B

Next, we used different concentrations of MODAG-009 and MODAG0005, anle138b and ACI-12589 to evaluate their affinity for MAO-B using [^{3}H]L-deprenyl displacement assay (n=3; **Fig 3a**). According to the one-site fitting model, MODAG-009 resulted in a displacement of more than 85% at 1 μM and an affinity of 216 nM (R^2=0.8329) for MAO-B (**Fig 3b**). MODAG-005 showed a displacement of more than 75% at 1 μM and an affinity of 204 nM (R^2 = 0.7259) for MAO-B (**Fig 3c**). Anle138b showed a displacement of more than 30% at 1 μM and an affinity of 64.3 nM (R^2=0.9190) for MAO-B (**Fig 3d**). In comparison, the ACI-12589 exhibited a displacement of 50% at 1 μM and an affinity of 368 nM (R^2= 0.8274) for MAO-B (**Fig 3e**).

***In vivo* [^{18}F]FD4 imaging revealed no off-target binding to MAO-B**

One patient with MSA were included in in vivo PET study. Their baseline demographic and clinical characteristics are summarized in STable 1. Visual assessment of paired [^{18}F]FD4 PET images revealed no apparent changes in the spatial distribution or regional intensity of tracer retention after 1 month of rasagiline treatment in the patient. Consistent with these findings, subtraction images generated by subtracting the baseline SUVR images from the corresponding post-rasagiline SUVR images revealed no prominent regional changes in [^{18}F]FD4 retention (**Fig 3a**).

Regional SUVR analysis revealed only small changes in [^{18}F]FD4 retention across the predefined brain regions (**Fig 3b**). In the MSA patient, regional changes ranged from −4.87% in the globus pallidus to +3.26% in the middle cerebellar peduncle. No marked regional increase or decrease in the [**^{18}F**]FD4 SUVR was observed after rasagiline treatment in either patient.

Discussion

As MAO-B is upregulated in reactive astrocytes across PD, DLB, and MSA, this off-target activity has the potential to confound the interpretation of *in vivo* PET signals, especially in regions with relatively abundant MAO-B expression. Our results indicate a clear divergence among the current αSyn ligand candidates. [^{18}F]FD4[11], C05-05[9] and [^{18}F]ACI-12589[6] has the reported affinity to αSyn of 2.59 nM, 1.5 nM and 33.5 nM. Here we showed that FD4[11] and C05-05[9] show no evidence of MAO-B binding. Our

finding is in line with an earlier report that C05-05 was insensitive to MAO-B[22]. Moreover, we found that ACI-12589 had a displacement of [^{3}H]L-deprenyl for approximately 50% at 1 μM and an affinity of 368nM (R^2= 0.8274) for MAO-B (**Fig 3e**). This is partly in line with the ex vivo evaluation and first-in-human study of [^{18}F]ACI-12589, showing no change in [^{18}F]ACI-12589 signal in MSA cases after complete MAO-B blocking with selegiline 10 mg for 6 days[6].

Anle138b-derived tracer [^{11}C]MODAG-005 of diarylpyrazole scaffolds was recently validated as a selective αSyn PET tracer in preclinical models, human brain tissue, and first-in-human MSA and PD imaging[8], with reported 0.2 nM affinity (binding potential (BP) of 33) to α-syn, and approximately 100-fold selectivity over tau and >1,000-fold over Aβ *in vitro*. MODAG-009 is an 18F analog of [^{11}C]MODAG-005. Here we found that MODAG-009 and MODAG-005[8] displaced [^{3}H]L-deprenyl in a concentration-dependent manner, showed over 85% and 75% off-target binding to MAO-B at 1 μM, whereas as anle138b showed 30% displacement at 1 μM, suggesting a much weaker MAO-B interaction. Further analysis showed the affinity for MODAG-009 (K_i=216 nM) and MODAG-005 (Ki=204 nM, i.e. IC50 = 416 nM) to MAO-B, which approximately in range with the reported IC50 of 0.8 μM for [^{11}C]MODAG-005[8].

Earlier study on MAO-B off-target binding for tau tracers, has shown that this pattern is specifically associated with certain chemical scaffolds[14], such as quinoline-based scaffolds[14] or specific pharmacophore features. The majority of 2nd-generation [^{18}F]flortaucipir-derivative tracers ([^{18}F]MK-6240, [^{18}F]RO-948, [^{18}F]PI-2620, and [^{18}F]GTP1) and the PBB3/florzolotau series do not show MAO-B off-target binding[14]. Whereas the 1st-generation quinoline based [^{18}F]THK-5351, and the 2nd-generation tau tracer quinoline-derived [^{18}F]JNJ-067 showed clear off-target binding to MAO-B[23] in postmortem brain and/or in silico. [^{18}F]THK-5351 has Kd of 2.9 nM, calculated BP=127 in AD brain for tauopathy[24], an IC50 of 780 nM (enzyme activity assays for MAO-B)[25]. *In vivo* PET study in humans study showed that selegiline reduced [^{18}F]THK5351 uptake about 85% in basal ganglia, 60–75% in cortex and 55% in cerebellum[25, 26]. Given that MAO-B is of high abundance in the brain (e.g. Bmax = 606 pmol/g tissue from [27]**)** and α-syn is of relatively low abundance compared to amyloid and tau, even moderate affinity matters for image interpretation. As MODAG-009 and MODAG-005 showed

measurable displacement of [^{3}H]L-deprenyl in cortical tissue *in vitro*, raising the same concern that PET signals attributed to αSyn could, in brain regions with a large number of MAO-B binding sites such as the striatum and brainstem or diseases marked by reactive astrogliosis (common in PD, DLB, and MSA). For MSA with very dense α-syn pathology, the influence might be low e.g. below 10 %, however in PD or DLB cases with sparse pathology BP <2, the influence might be 30% or higher.

There are several limitations in this study. The sample size of the *in vivo* blocking study in patients was small and that only [^{18}F]FD4 was available for evaluation. 2) We did not assess the MAO-B binding using enzyme assays, in silico modeling or *in vivo* animal imaging approaches. 3) Moreover, we did not use the striatum tissue from MSA or PD patients to study off-target binding to MAO-B. Further displacement studies and in silico studies are needed to quantify the affinity of the tracer for MAO-B relative to α-syn. Additionally, labeled α-syn tracer allows the assessment of the MAO-B-to-α-syn ratio of each tracer in both *in vitro* and *in vivo* setting, such as in selegiline- or rasagiline-blocking PET.

In conclusion, our data indicate that the diarylpyrazole-scaffold based α-syn ligands tested here show measurable binding to MAO-B. This off-target interaction should be considered when interpreting *in vivo* imaging patterns, particularly in regions with high MAO-B expression. Further characterization of tracer selectivity, together with *in vivo* blocking studies, will help define the contribution of MAO-B to α-syn binding in PET signal.

Competing interests

The authors have no competing interests. KS, AR and RN are editorial board members of EJNMMI.

Funding

RN received funding from UNIBE Forschungsstiftung, Peter Bockhoff Stiftung and Novartis Foundation for Medical-biological Research. CZ received funding from the Shanghai Science and Technology Program Project (25TS1405000), a grant (No.82394434) from the National Natural Science

Foundation of China, and the Shanghai Municipal Science and Technology Major Project. QJ received funding from China Scholarship Council (202606100174).

Authors' contributions

RN and CZ conceived and designed the study. CZ, FL, JW, and QJ recruited patients, collected *in vivo* data and performed data analysis. SZ performed the synthesis and QC of the chemicals. MW performed the autoradiography and *in vitro* data analysis, and DG performed the staining and microscopy. MW and QJ prepared the figures. MW, QJ and RN wrote the first draft. All the authors contributed to the revision of the manuscript. All the authors read and approved the final manuscript.

Acknowledgments

The authors would like to thank the Microscopy Imaging Center at the University of Bern and ZMB for technical assistance.

Data availability

Data is available upon request.

Reference

(1) Lin, H.; Zhang, Y.; Zhao, Y.; Wei, Y.; Combes, B. F.; Henrich, M. T.; Geibl, F. F.; Oertel, W. H.; Shi, K.; Rominger, A.; et al. Multimodal neuroimaging elucidates the posterior-to-anterior gradient of nigrostriatal degeneration in Parkinson's disease. *NPJ Parkinsons Dis* **2026**. DOI: 10.1038/s41531-026-01456-y From NLM.

(2) Höglinger, G. U.; Adler, C. H.; Berg, D.; Klein, C.; Outeiro, T. F.; Poewe, W.; Postuma, R.; Stoessl, A. J.; Lang, A. E. A biological classification of Parkinson's disease: the SynNeurGe research diagnostic criteria. *Lancet Neurol* **2024**, *23* (2), 191-204. DOI: 10.1016/s1474-4422(23)00404-0 From NLM.

(3) Simuni, T.; Chahine, L. M.; Poston, K.; Brumm, M.; Buracchio, T.; Campbell, M.; Chowdhury, S.; Coffey, C.; Concha-Marambio, L.; Dam, T.; et al. A biological definition of neuronal α-synuclein disease: towards an integrated staging system for research. *Lancet Neurol* **2024**, *23* (2), 178-190. DOI: 10.1016/s1474-4422(23)00405-2 From NLM.

(4) Dubois, B.; Villain, N.; Frisoni, G. B.; Rabinovici, G. D.; Sabbagh, M.; Cappa, S.; Bejanin, A.; Bombois, S.; Epelbaum, S.; Teichmann, M.; et al. Clinical diagnosis of Alzheimer's disease: recommendations of the International Working Group. *The Lancet Neurology* **2021**, *20* (6), 484-496. DOI: https://doi.org/10.1016/S1474-4422(21)00066-1.

(5) Pees, A.; Grotegerd, A. K.; Bleher, D.; Herfert, K.; Vasdev, N. PET imaging of alpha-synuclein: from radiotracer design through in vitro and in vivo translation. *Eur J Nucl Med Mol Imaging* **2026**, *53* (6), 4211-4239. DOI: 10.1007/s00259-025-07695-0 From NLM.

(6) Smith, R.; Capotosti, F.; Schain, M.; Ohlsson, T.; Vokali, E.; Molette, J.; Touilloux, T.; Hliva, V.; Dimitrakopoulos, I. K.; Puschmann, A.; et al. The α-synuclein PET tracer [18F] ACI-12589 distinguishes multiple system atrophy from other neurodegenerative diseases. *Nat Commun* **2023**, *14* (1), 6750. DOI: 10.1038/s41467-023-42305-3 From NLM.

(7) Xiang, J.; Tao, Y.; Xia, Y.; Luo, S.; Zhao, Q.; Li, B.; Zhang, X.; Sun, Y.; Xia, W.; Zhang, M.; et al. Development of an α-synuclein positron emission tomography tracer for imaging synucleinopathies. *Cell* **2023**, *186* (16), 3350-3367.e3319. DOI: 10.1016/j.cell.2023.06.004 From NLM.

(8) Saw, R. S.; Haas, S.; Schmidt, F.; Ryazanov, S.; Leonov, A.; Bleher, D.; Grotegerd, A. K.; Kuebler, L.; Roeben, B.; Reimold, M.; et al. The PET tracer [(11)C]MODAG-005 targets alpha-synuclein aggregates in the brain. *Sci Transl Med* **2026**, *18* (851), eaec0813. DOI: 10.1126/scitranslmed.aec0813 From NLM.

(9) Endo, H.; Ono, M.; Takado, Y.; Matsuoka, K.; Takahashi, M.; Tagai, K.; Kataoka, Y.; Hirata, K.; Takahata, K.; Seki, C.; et al. Imaging α-synuclein pathologies in animal models and patients with Parkinson's and related diseases. *Neuron* **2024**, *112* (15), 2540-2557.e2548. DOI: 10.1016/j.neuron.2024.05.006 From NLM.

(10) Goto, R.; Matsuoka, K.; Kimura, Y.; Kataoka, Y.; Oya, M.; Hirata, K.; Tagai, K.; Takahata, K.; Seki, C.; Kawamura, K.; et al. Human biodistribution and radiation dosimetry of two novel α-synuclein PET tracers, (18)F-SPAL-T-06 and (18)F-C05-05. *Sci Rep* **2025**, *15* (1), 8640. DOI: 10.1038/s41598-025-93520-5 From NLM.

(11) Liang, Q.; Wang, J.; Zuo, C.; Liu, C.; Li, D.; Liu, F.; Ge, J.; Lu, J.; Yang, Y.; Bian, J.; et al. Human Imaging and IND-Enabling Studies for an α-Synuclein PET Tracer^{18}F-FD4 in Parkinson’s Disease (PD) and Multiple System Atrophy (MSA) Subtypes. *Journal of Nuclear Medicine* **2026**, *67* (supplement 1), 262109.

(12) Saturnino Guarino, D.; Crosby, J.-G.; Sessions, Z. L.; Dhavale, D. D.; Robinson, J. L.; Schuck, T.; Lee, E. B.; Kotzbauer, P. T.; Luk, K. C.; Lee, V. M. Y.; et al. New PET ligand 3H-M503-1619 captures α-synuclein in human postmortem LBDs but not in MSA tissue. *npj Parkinson's Disease* **2026**. DOI: 10.1038/s41531-026-01564-9.

(13) Tian, G. L.; Hsieh, C. J.; Guarino, D. S.; Graham, T. J. A.; Lengyel-Zhand, Z.; Schmitz, A.; Chia, W. K.; Young, A. J.; Crosby, J. G.; Plakas, K.; et al. The development of a PET radiotracer for imaging alpha synuclein aggregates in Parkinson's disease. *RSC Med Chem* **2025**. DOI: 10.1039/d5md00057b From NLM.

(14) Higuchi, M.; Tagai, K.; Takahata, K.; Endo, H. Advances in PET imaging of protein aggregates associated with neurodegenerative disease. *Nat Rev Neurol* **2025**, *21* (9), 506-522. DOI: 10.1038/s41582-025-01126-2 From NLM.

(15) Ni, R. PET imaging in animal models of Parkinson's disease. *Behavioural Brain Research* **2022**, 114174. DOI: https://doi.org/10.1016/j.bbr.2022.114174.
(16) Ni, R.; Röjdner, J.; Voytenko, L.; Dyrks, T.; Thiele, A.; Marutle, A.; Nordberg, A. In vitro Characterization of the Regional Binding Distribution of Amyloid PET Tracer Florbetaben and the Glia Tracers Deprenyl and PK11195 in Autopsy Alzheimer's Brain Tissue. *J Alzheimers Dis* **2021**, *80* (4), 1723-1737. DOI: 10.3233/jad-201344 From NLM.
(17) Marutle, A.; Gillberg, P.-G.; Bergfors, A.; Yu, W.; Ni, R.; Nennesmo, I.; Voytenko, L.; Nordberg, A. 3 H-Deprenyl and 3 H-PIB autoradiography show different laminar distributions of astroglia and fibrillar β-amyloid in Alzheimer brain. *Journal of neuroinflammation* **2013**, *10* (1), 1-15.
(18) Rodriguez-Vieitez, E.; Ni, R.; Gulyás, B.; Tóth, M.; Häggkvist, J.; Halldin, C.; Voytenko, L.; Marutle, A.; Nordberg, A. Astrocytosis precedes amyloid plaque deposition in Alzheimer APPswe transgenic mouse brain: a correlative positron emission tomography and in vitro imaging study. *Eur J Nucl Med Mol Imaging* **2015**, *42* (7), 1119-1132. DOI: 10.1007/s00259-015-3047-0 From NLM.
(19) Kong, Y.; Maschio, C. A.; Shi, X.; Xie, F.; Zuo, C.; Konietzko, U.; Shi, K.; Rominger, A.; Xiao, J.; Huang, Q.; et al. Relationship Between Reactive Astrocytes, by [(18)F]SMBT-1 Imaging, with Amyloid-Beta, Tau, Glucose Metabolism, and TSPO in Mouse Models of Alzheimer's Disease. *Mol Neurobiol* **2024**. DOI: 10.1007/s12035-024-04106-7 From NLM.
(20) Wenning, G. K.; Stankovic, I.; Vignatelli, L.; Fanciulli, A.; Calandra-Buonaura, G.; Seppi, K.; Palma, J. A.; Meissner, W. G.; Krismer, F.; Berg, D.; et al. The Movement Disorder Society Criteria for the Diagnosis of Multiple System Atrophy. *Mov Disord* **2022**, *37* (6), 1131-1148. DOI: 10.1002/mds.29005 From NLM.
(21) Xiao, Y.; Lau, J. C.; Anderson, T.; DeKraker, J.; Collins, D. L.; Peters, T.; Khan, A. R. An accurate registration of the BigBrain dataset with the MNI PD25 and ICBM152 atlases. *Sci Data* **2019**, *6* (1), 210. DOI: 10.1038/s41597-019-0217-0 From NLM.
(22) Matarazzo, M.; Obeso, J. A. Alpha synuclein PET imaging, a step closer to in vivo neuropathology in Parkinson's disease and related disorders. *Neuron* **2024**, *112* (15), 2457-2458. DOI: 10.1016/j.neuron.2024.07.001 From NLM.
(23) Chun, H.; Youn, W.; Lim, H.; Harada, R.; Ko, H. Y.; Yoon, J.; Oh, S. J.; Seemann, P.; Pepe, J. G.; Shoichet, B. K.; et al. In-depth multimodal validation of (18)F-THK5351 for imaging monoamine oxidase-B-mediated reactive astrogliosis in Alzheimer's and related neurodegenerative diseases. *Exp Mol Med* **2026**, *58* (7), 2123-2137. DOI: 10.1038/s12276-026-01757-5 From NLM.
(24) Harada, R.; Okamura, N.; Furumoto, S.; Furukawa, K.; Ishiki, A.; Tomita, N.; Tago, T.; Hiraoka, K.; Watanuki, S.; Shidahara, M.; et al. 18F-THK5351: A Novel PET Radiotracer for Imaging Neurofibrillary Pathology in Alzheimer Disease. *J Nucl Med* **2016**, *57* (2), 208-214. DOI: 10.2967/jnumed.115.164848 From NLM.
(25) Chun, H.; Youn, W.; Lim, H.; Harada, R.; Ko, H. Y.; Yoon, J.; Oh, S.-J.; Seemann, P.; Pepe, J. G.; Shoichet, B. K.; et al. In-depth multimodal validation of 18F-THK5351 for imaging monoamine oxidase-B-mediated reactive astrogliosis in Alzheimer's and related neurodegenerative diseases. *Experimental & Molecular Medicine* **2026**, *58* (7), 2123-2137. DOI: 10.1038/s12276-026-01757-5.
(26) Ng, K. P.; Pascoal, T. A.; Mathotaarachchi, S.; Therriault, J.; Kang, M. S.; Shin, M.; Guiot, M. C.; Guo, Q.; Harada, R.; Comley, R. A.; et al. Monoamine oxidase B inhibitor, selegiline, reduces 18F-THK5351 uptake in the human brain. *Alzheimer's Research and Therapy* **2017**, *9* (1). DOI: 10.1186/s13195-017-0253-y.
(27) Villemagne, V. L.; Harada, R.; Doré, V.; Furumoto, S.; Mulligan, R.; Kudo, Y.; Burnham, S.; Krishnadas, N.; Bozinovski, S.; Huang, K.; et al. First-in-Humans Evaluation of (18)F-SMBT-1, a Novel (18)F-Labeled Monoamine Oxidase-B PET Tracer for Imaging Reactive Astrogliosis. *J Nucl Med* **2022**, *63* (10), 1551-1559. DOI: 10.2967/jnumed.121.263254 From NLM.

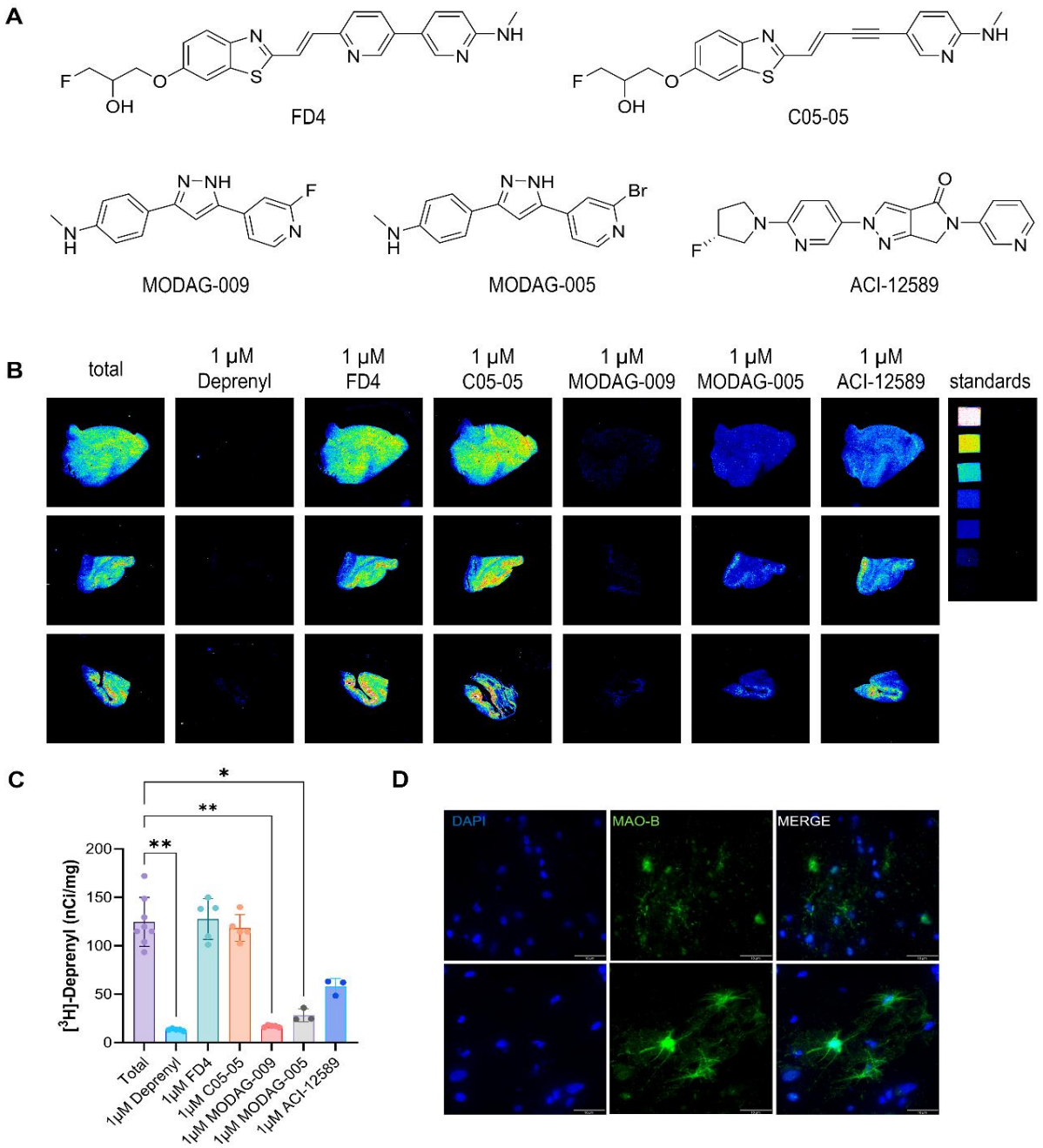

Figure 1: Diverse off-targeting binding to MAO-B with different a-synuclein ligands. A) Chemical structures of a-synuclein ligands. B) [³H]L-deprenyl autoradiography in the frontal cortex under total-binding, R-(-)-deprenyl hydrochloride-block, and 1 µM competition (FD4, C05-05, MODAG-009, MODAG-005, and ACI-12589) conditions. Color bar = 489.1 nCi/mg, 243.0 nCi/mg , 138.1 nCi/mg, 63.1 nCi/mg, 36.3 nCi/mg, 16.6 nCi/mg, 8.0 nCi/mg, 3.7 nCi/mg, 2.0 nCi/mg, 1.04 nCi/mg, 0.54 nCi/mg, 0.29 nCi/mg, 0.14 nCi/mg, 0.00 nCi/mg). C) Quantified [³H]L-deprenyl binding (nCi/mg) across conditions (mean ± SD, n=5 cases); * $p < 0.05$, ** adjusted $P < 0.01$ vs. total. One-way repeated-

measures ANOVA with Dunnett's multiple comparisons was used. D) MAO-B immunofluorescence staining on the postfixed frozen human brain slice to the adjacent frozen slice for autoradiography. DAPI (blue), MAO-B (green). Scale bar=10μm.

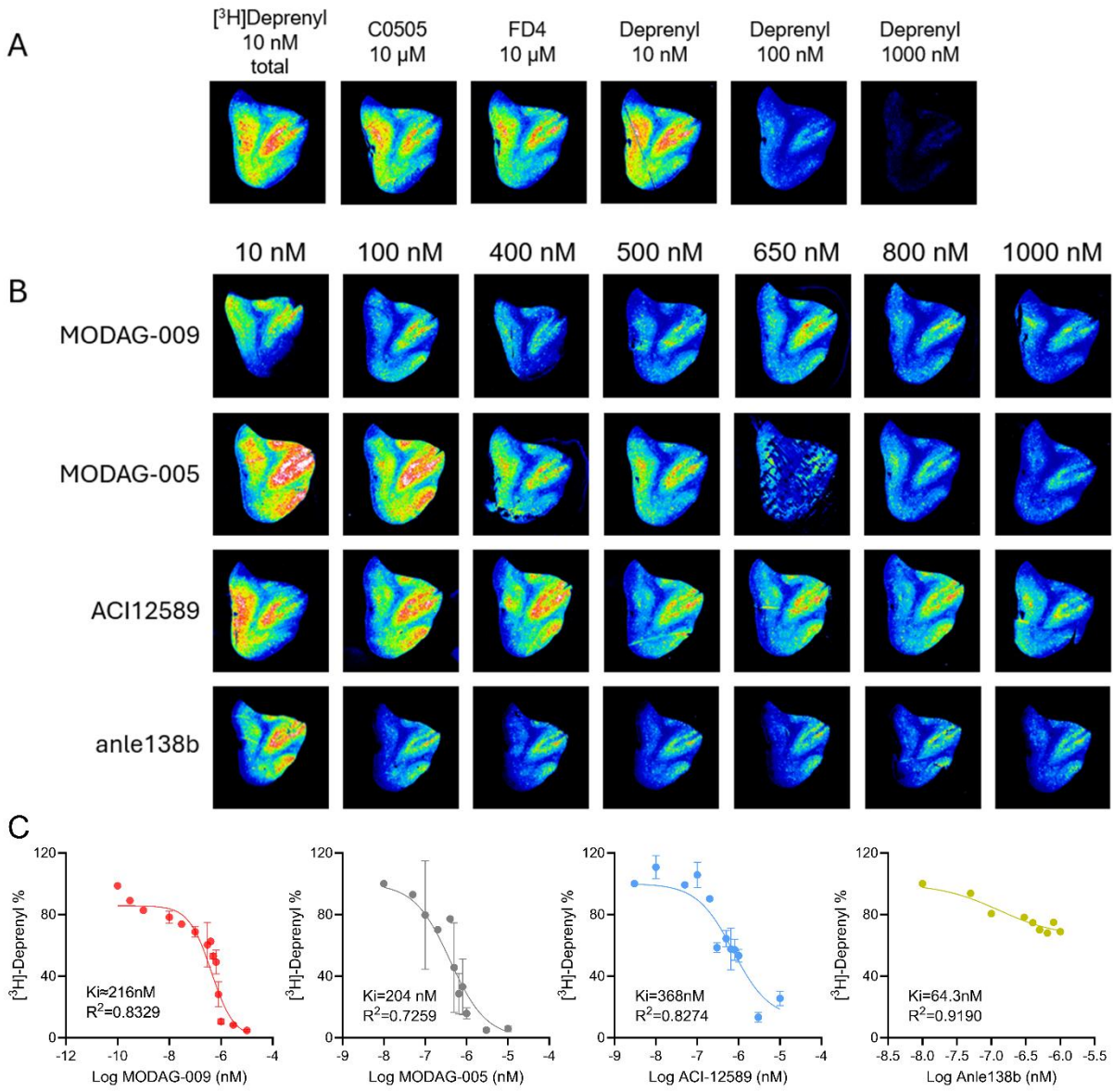

Figure 2 Displacement evaluation of MODAG-009, MODAG-005, anle138b and ACI-12589 to MAO-B. A) Representative autoradiographic images showing [³H]L-Deprenyl binding in the absence (total binding) or presence of increasing concentrations of unlabeled Deprenyl (10-1000 nM), as well as C05-05 and FD4 (10 µM each) on the frontal cortex tissue. B) Representative autoradiographic images illustrating the concentration-dependent displacement of [³H]L-Deprenyl binding by MODAG-009, MODAG-005, ACI-12589, and anle138b (10-1000 nM). Color-coded signal intensities represent relative radioligand binding, with red/yellow indicating higher binding and blue/black indicating lower binding. C) Competition binding curves were generated by plotting the percentage of [³H]L-Deprenyl binding relative to total binding against the logarithm of competitor concentration (nM). The calculated

inhibition constants (K_i) were 216 nM for MODAG-009, 204 nM for MODAG-005, 368 nM for ACI-12589, and 64.3 nM for anle138b. The corresponding coefficients of determination (R^2) are indicated in each graph.

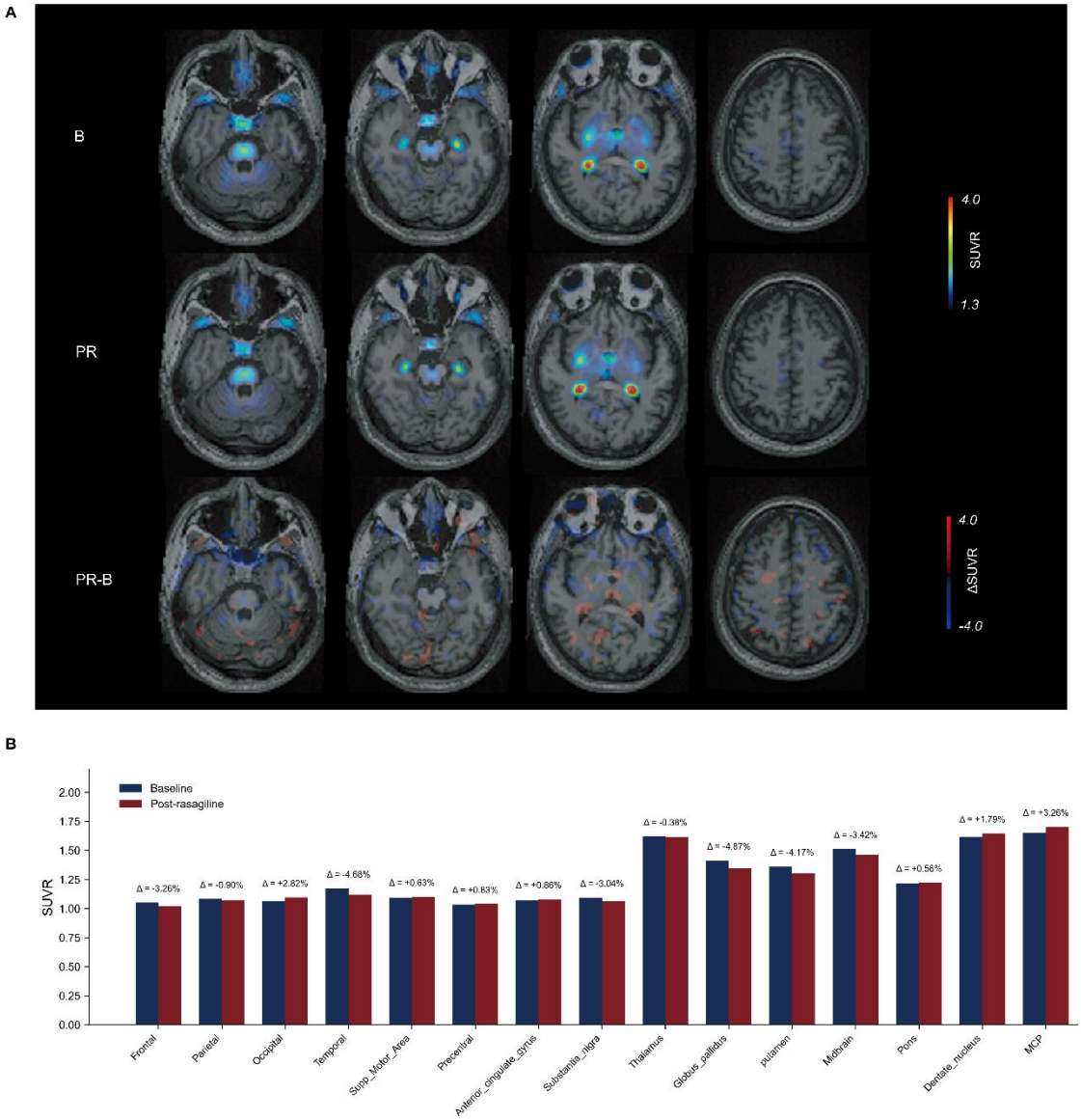

Figure 3. Chronic rasagiline challenge did not affect [^{18}F]FD4 retention in the brains of the patient with MSA. (A) For each patient, [^{18}F]FD4 PET images at baseline, post-rasagiline, and subtraction (post-rasagiline minus baseline) are displayed from the rostral to caudal direction. (B) Regional [^{18}F]FD4 SUVRs before and after rasagiline treatment in the patient with MSA. Cerebellar gray matter was used as the reference region for the SUVR calculations. B, baseline; PR, post-rasagiline; PR-B, post-rasagiline minus baseline; SUVR, standardized uptake value ratio.

STable 1. Baseline demographic and clinical characteristics of the MSA participant for *in vivo* [^{18}F]FD4 PET.

	Patient
Diagnosis	MSA
Age (years)	55
Sex	Male
Education (years)	20
Disease duration (months)	26
LEDD at baseline (mg)	250
UPDRS	69
HY	4
MoCA-B	22
UMSARS I	28
UMSARS II	27
UMSARS I+II	55
UMSARS III	1
UMSARS IV	4

Abbreviations: MSA, multiple system atrophy; LEDD, levodopa equivalent daily dose; UPDRS, unified Parkinson's disease rating scale; HY, Hoehn–Yahr staging scale; MoCA-B, the Chinese version of the Montreal Cognitive Assessment-B; UMSARS, unified multiple system atrophy rating scale.

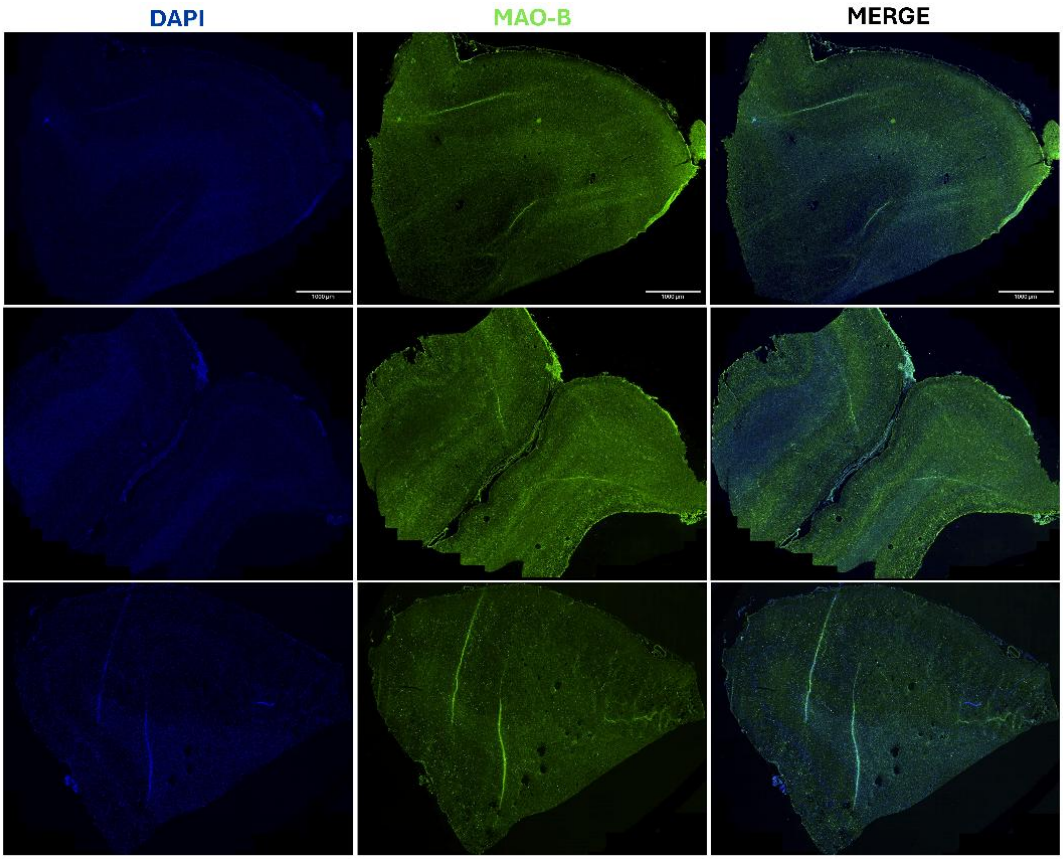

SFig 1. MAO-B immunofluorescence staining on the postfixed frozen human brain slice to the adjacent frozen slice for autoradiography. DAPI (blue), MAO-B (green). Scale bar=1 mm

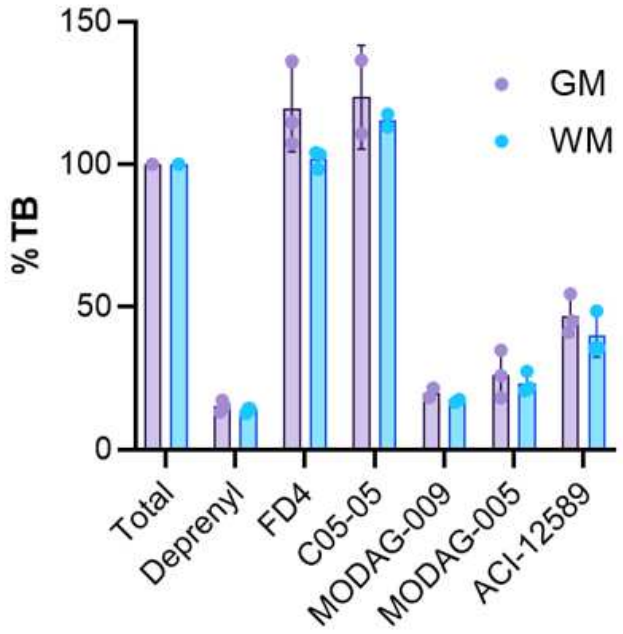

SFig 2. **Displacement of binding to MAO-B with different a-synuclein ligands in grey and white matter of cortex.** %Total Binding (%TB) of 1 μM competition (FD4, C05-05, MODAG-009, MODAG-005, and ACI-12589) separated into grey and white matter.